Available online at www.sciencedirect.com
ScienceDirect
Catalysis Today 122 (2007) 352–360
CATALYSIS TODAY
www.elsevier.com/locate/cattod

Au^0 nanocolloids as recyclable quasihomogeneous metal catalysts in the chemoselective hydrogenation of α,β-unsaturated aldehydes and ketones to allylic alcohols

P.G.N. Mertens [a], H. Poelman [b], X. Ye [c], I.F.J. Vankelecom [a], P.A. Jacobs [a], D.E. De Vos [a,*]

[a] K.U. Leuven, Centre for Surface Chemistry and Catalysis, Kasteelpark Arenberg 23, 3001 Heverlee, Belgium
[b] Ghent University, Department of Solid State Sciences, Krijgslaan 281, S1, 9000 Gent, Belgium
[c] K.U. Leuven, Department of Metallurgy and Materials Engineering, Kasteelpark Arenberg 44, 3001 Heverlee, Belgium

Available online 2 April 2007

Abstract

In the catalytic hydrogenation of α,β-unsaturated aldehydes and ketones, highly selective allylic alcohol formation can be achieved by application of Au^0 nanocolloids dispersed in amide solvents. The polyvinylpyrrolidone protected Au^0 nanoparticles prefer C=O reduction over C=C saturation and act as chemoselective quasihomogeneous metal catalysts in the hydrogenation of *trans*-2-butenal (crotonaldehyde), 2-methyl-2-propenal (methacrolein), 4-methyl-3-penten-2-one (mesityl oxide) and 3-methyl-3-penten-2-one. An extensive solvent screening revealed the superiority of amides as media for both synthesis and application of the Au^0 nanocolloids. In comparison with the widely used alcohol solvents, amides offer enhanced colloidal stability for the Au^0 nanosol and increased hydrogenation chemoselectivity. Control over the Au^0 cluster formation provided the opportunity to investigate the size-dependency of the catalytic performance and to determine the optimum gold cluster size for a maximization of the allylic alcohol yields. The most successful Au^0 clusters, with a typical diameter of 7 nm and synthesized in *N*,*N*-dimethylformamide, lead to a crotyl alcohol selectivity of 73% at 93% crotonaldehyde conversion and a 58% allylic alcohol yield in the hydrogenation of mesityl oxide at a molar substrate/Au catalyst ratio of 200. Analogous Pt^0 and Ru^0 sols are more active than the Au^0 nanosols, but substantially less chemoselective for allylic alcohols. The Au^0 nanocolloids can be recycled efficiently by ultrafiltration over custom-made, cross-linked polyimide membranes. In the recycling experiments the gold nanodispersion was well retained by the solvent-resistant ultrafiltration membranes and the performance of the colloidal gold catalyst was satisfactorily preserved in successive hydrogenation runs.

Keywords: Hydrogenation; Unsaturated aldehyde; Unsaturated ketone; Allylic alcohol; Colloidal catalyst; Quasihomogeneous catalyst; Solvent-resistant ultrafiltration; Gold

1. Introduction

The chemoselective hydrogenation of α,β-unsaturated aldehydes and ketones attracts much interest in catalysis research since allylic alcohols are valuable intermediates in the production of various fine chemical, pharmaceutical and cosmetic compounds [1–3]. In the intramolecular competition between saturation of the olefinic bond and the reduction of the carbonyl group (Scheme 1), the C=C hydrogenation is thermodynamically favored. As the kinetics of the hydrogenation strongly depend on the applied metal catalyst the obvious challenge for catalytic chemists is to open a kinetically favored path to the allylic alcohol by the development of an appropriate hydrogenation metal catalyst. Additionally, the type and degree of substitution on both the carbonyl group and the olefinic bond strongly affect the chemoselectivity of the hydrogenation.

Heterogeneous gold nanocatalysts have been proven to activate H_2, and have successfully been applied to the selective hydrogenation of polyunsaturated compounds like alkadienes and aromatic nitro compounds [4–8]. Regarding the use of Au catalysts in the hydrogenation of α,β-unsaturated carbonyl compounds, most reports have focused on unsaturated aldehydes such as acrolein, crotonaldehyde or citral [9–16]. The more challenging chemoselective hydrogenation of α,β-unsaturated ketones like mesityl oxide has been studied only occasionally [17–19]. In all these studies heterogeneous Au

* Corresponding author. Tel.: +32 16 321639; fax: +32 16 321998.
E-mail address: Dirk.DeVos@biw.kuleuven.be (D.E. De Vos).

0920-5861/$ – see front matter © 2007 Elsevier B.V. All rights reserved.
doi:10.1016/j.cattod.2007.02.021

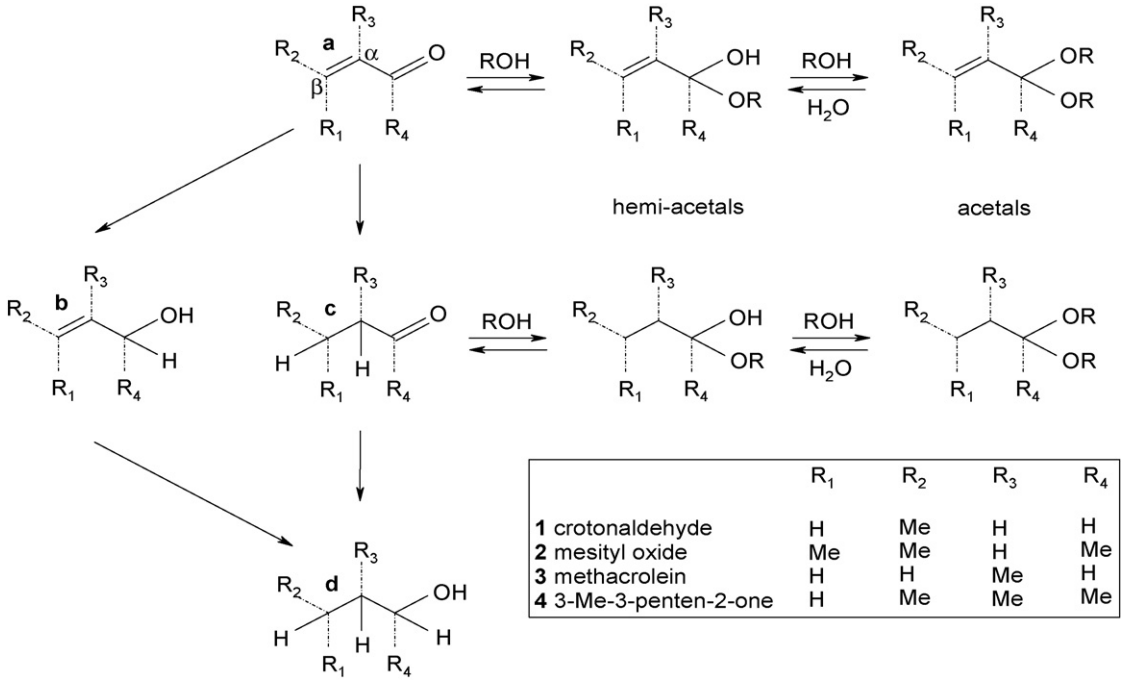

	R1	R2	R3	R4
1 crotonaldehyde	H	Me	H	H
2 mesityl oxide	Me	Me	H	Me
3 methacrolein	H	H	Me	H
4 3-Me-3-penten-2-one	H	Me	Me	Me

Scheme 1. Transformation of α,β-unsaturated aldehydes and ketones.

catalysts have been used, in which Au is usually dispersed on a Lewis acid support.

As a consequence, the intrinsic catalytic performance of Au and its size-dependency cannot accurately be derived from the previous investigations: in each case the Au catalyst's performance is influenced by the support. If one aims at examining the catalytic properties of unpromoted, unsupported Au, the use of stable metallic sols is an attractive option. Aqueous gold nanosols have already found application in the selective oxidation of alcohols [20–23], but Au sols have not yet been applied in hydrogenations. Previous work on the chemoselective C=O hydrogenation catalyzed by metallic sols was based on other metals, e.g. Pt or Ru nanocolloids stabilized by polyvinylpyrrolidone, requiring Lewis acid promotion to obtain high yields of unsaturated alcohol [24–26].

In this study, we investigate the application of Au^0 nanocolloids in the hydrogenation of challenging substrates like crotonaldehyde and mesityl oxide. The objective is an unpromoted chemoselective Au^0 catalyst leading to high yields of allylic alcohol. The effects of the gold precursor and the organic solvent on the Au^0 nanosol synthesis and the ensuing chemoselective hydrogenation are assessed. Moreover the effects of alkyl substituents on the C=O and C=C bonds of the α,β-unsaturated carbonyl substrates on the hydrogenation rate and chemoselectivity are examined. Finally, recycling of the Au^0 nanocolloids by ultrafiltration over custom-made polymer membranes is investigated. This filtration technique already proved successful in the separation of polyvinylalcohol protected Au^0 nanocolloids from alcoholic reaction mixtures [21,22]. The solvent stability of organic membranes during filtration is of particular importance and might require a specific cross-linking post-synthesis treatment of the membrane, e.g. when polyimide membranes are applied in amide solvents [27].

2. Experimental

2.1. Catalyst preparation and characterization

The Au^0 colloids were synthesized by adding 0.2 mmol of $AuCl_3$ or $HAuCl_4{\cdot}3H_2O$ (Acros) to 8 mL of a stirred alcohol or amide solution containing 0.033, 0.067, 0.100, 0.133, 0.200, 0.300 or 0.400 g polyvinylpyrrolidone (MW = 10.000, PVP-10, Sigma–Aldrich). The applied PVP variations lead to molar ratios of PVP monomers to Au of 1.5, 3, 4.5, 6, 9, 13.5 and 18, respectively. After 12 h at 298 K, 2 mL of an alcohol or amide solution containing 1 mmol of dissolved $NaBH_4$ was added (molar ratio metal chloride/$NaBH_4$ = 1/5) to generate the final Au^0 sol. As synthesis solvents, the alcohols ethanol, 2-propanol and 2-butanol were applied next to amides like *N*,*N*-dimethylacetamide (DMA) and *N*,*N*-dimethylformamide (DMF). The same solvent was used for dissolving the Au precursor and the hydride reducing agent. Likewise Pt^0 and Ru^0 sols were generated with, respectively, K_2PtCl_4 and $RuCl_3{\cdot}xH_2O$ as the metal precursors.

For transmission electron microscopy characterization 0.1 mL of the Au^0 sol was dispersed in 0.9 mL ethanol. Droplets containing the Au^0 colloids were mounted on a carbon film supported on a copper grid, with subsequent drying at ambient conditions. The TEM images were recorded on a Philips CM20 electron microscope, operating at 200 kV. The average size of the Au^0 particles, d_{Au}, was obtained by calculating the number average diameter for an ensemble of 100 Au particles observed in TEM.

The Au^0 sols were additionally characterized by UV–vis Spectroscopy using a Perkin Elmer Lambda 12 spectrophotometer. This technique can detect the Surface Plasmon Resonance (SPR) band which is conclusive evidence for the

presence of gold as zerovalent nanoparticles. In addition particle size variations between the various Au^0 sols can be observed by the shift in SPR wavelength position in the absorption spectrum [28,29]. For characterization the Au^0 sols were diluted with the appropriate solvent to 1/20 of the original gold content.

In addition 0.2 mL of a gold sol was immobilized on a glass slide to permit characterization by X-ray Photoelectron Spectroscopy in a Perkin Elmer Phi ESCA 5500 apparatus equipped with a monochromated 450 W Al Kα source. Wide scan spectra were measured over a binding energy range of 0–600 eV with a 187.85 eV pass energy. The Na1s (1069 eV), Au4f (84 eV), O1s (530 eV) and C1s (284.6 eV; taken as binding energy reference) levels were recorded in separate high resolution energy windows, while the B1s (191 eV) and Cl2p (197.5 eV) signals were measured together in one energy window. The pass energy for these multiplex windows was 58.70 eV. The XPS data analysis was performed with the Multipak V6.1A program.

2.2. Membrane synthesis and characterization

The polyimide (PI, Matrimid 9725 US, Huntsman, Switzerland) was dried overnight at 403 K prior to use. A 15 wt.% polymer solution was prepared by dissolving the Matrimid powder in a solvent mixture of *N*-methylpyrrolidone as a solvent, tetrahydrofuran as a volatile co-solvent and 2 wt.% deionized H_2O as a non-solvent additive. The *N*-methylpyrrolidone/tetrahydrofuran weight ratio was set at 3/1. This polymer solution was stirred for 12 h and subsequently the obtained homogeneous solution was cast on a polypropylene/polyethylene support (FO 2471, Viledon, Germany) by means of an automatic film applicator (Braive Instruments, Belgium). The cast speed and film thickness amounted to 1.2 m/min and 250 μm, respectively. Solvents were allowed to evaporate during 30 s; the nascent film was then immersed in deionized H_2O for 1 h. Subsequently the membrane was treated by solvent exchange and kept for 3 h in 2-propanol, followed by 72 h in a 40 vol.% 2-propanol solution of glycerol.

Afterwards the polyimide (PI) membrane was modified by a chemical cross-linking procedure to enhance its chemical stability in polar aprotic solvents like amides. Therefore the polymer membrane was immersed in a cross-linking reagent bath, comprising 10 wt.% of *p*-xylylenediamine in methanol, for 12 h at 293 K. Next the membrane was washed with methanol to remove the excess reagent, after which it was kept in *N*,*N*-dimethylformamide prior to use in the recycling experiments.

For scanning electron microscopy, membrane cross-sections were obtained by breaking the polyimide membranes under liquid N_2. The samples were then coated with a Au layer to reduce the membrane charging under the electron beam. The SEM images were recorded with a Philips XL FEG 30 electron microscope.

To study the effect of the post-synthesis cross-linking treatment, PI membrane samples were additionally characterized by Diffuse Reflectance Infrared Fourier Transform Spectroscopy by means of a Nicolet 730-FT-IR spectrometer equipped with a Spectra-Tech DRIFTS apparatus. The PI membrane samples were immersed in the cross-linking solution for, respectively, 0.25, 3 and 12 h and compared with an untreated PI membrane. The cross-linked PI membranes were thoroughly rinsed with methanol to remove residual *p*-xylylenediamine and dried for 2 h at 348 K prior to characterization. The presence of N–H stretching vibrations in the wavenumber region around 3250 cm^{-1} was monitored since the cross-linking results in the substitution of imide groups (no N–H groups) by amidic bonds (N–H groups).

2.3. Hydrogenation experiment and analysis

A typical reaction mixture consisted of 0.5 mL alcohol or amide solvent, 0.5 mL alcoholic or amidic Au^0, Pt^0 or Ru^0 sol (equivalent with 0.01 mmol Au, Pt or Ru) and 1 or 2 mmol of an α,β-unsaturated carbonyl compound. Prior to addition of the substrates the diluted metal sols were pressurized to 4.0 MPa H_2 at 298 K for 1 h, in order to prevent any reoxidation of the metal catalyst [30]. As the substrate/metal ratio in the hydrogenation amounts to 200/1, and as the $NaBH_4$/metal ratio in the sol preparation is 5/1, the influence of residual $NaBH_4$ on the hydrogenation results can be neglected. The reaction mixtures were pressurized to 0.5–4.0 MPa H_2 and kept at 303–343 K while stirring at 1000 rpm for different reaction times. All reactions were performed in a high throughput mode by means of a multi-reactor unit (TOP Industries, France) containing 10 mini-reactors of 4 mL volume except for the catalyst recycling experiments for which a thermocontrolled autoclave was used.

For the analysis of the reaction samples, use was made of a gas chromatograph with a 0.32 mm i.d. by 50 m WCOT fused silica column coated with a Chrompack CP-WAX 58 CB stationary phase (1.2 μm d_f). The instrument was equipped with a FID detector. The retention times of potential hydrogenation products were compared with those of the commercial reference compounds *trans*-2-buten-1-ol (crotyl alcohol; **1b**), butanal (**1c**), 1-butanol (**1d**), 4-methyl-2-pentanone (**2c**), 4-methyl-2-pentanol (**2d**), methallyl alcohol (**3b**), 2-methyl-1-propanol (**3d**), 3-methyl-2-pentanone (**4c**) and 3-methyl-2-pentanol (**4d**). GC–MS analysis allowed to assign the remaining peak positions to 4-methyl-3-penten-2-ol (**2b**), 2-methyl-propanal (**3c**) and 3-methyl-3-penten-2-ol (**4b**). Additional corroboration of the identification of the allylic alcohols was obtained by chemoselective C=O reduction by means of the Luche protocol [31,32]. Peaks of possible acetalization products were assigned by acidifying alcoholic solutions of crotonaldehyde and mesityl oxide with HCl and analyzing these mixtures by GC–MS.

The conversion ($C_{\text{unsat carb.}}$, %) represents the molar fraction of initial α,β-unsaturated carbonyl compound converted to the various products. The selectivity ($S_{\text{all alc.}}$, %) represents in each case the fraction of the allylic alcohols, i.e. crotyl alcohol (**1b**), 4-methyl-3-penten-2-ol (**2b**), methallyl alcohol (**3b**), or 3-methyl-3-penten-2-ol (**4b**) in the pool of reaction products. The yield ($Y_{\text{all alc.}}$, %) is the percentual product of the substrate

conversion and the allylic alcohol selectivity. $S_{sat\ carb.}$ and $S_{sat\ alc.}$ represent the portion of, respectively, saturated carbonyl compounds and saturated alcohols. $S_{acetal.}$ stands for the extent of (hemi)acetalization product formation. Selectivities are mostly reported at high conversions, around 90%. Substrate reactivities and hydrogenation rates were derived from samples taken at conversion levels below 25%.

2.4. Catalyst recycling experiment

The recycling experiments comprised three successive hydrogenation runs, with two membrane filtrations in between. The filtrations were performed at 298 K applying a driving force of 1.0 MPa N_2. A 20 mL autoclave was filled with 4 mL of the Au^0 sol and 4 mL *N*,*N*-dimethylformamide. Prior to the addition of crotonaldehyde the diluted metal sol was pressurized to 4.0 MPa H_2 at 298 K for 1 h. Next 8 mmol of crotonaldehyde was added and the autoclave was pressurized to 4.0 MPa H_2 at 333 K for 24 h. After this first run, the composition was analyzed by removing an aliquot from the reaction mixture. The remainder of the solution was concentrated by filtration to a 4 mL volume containing the colloidal Au^0 catalyst. This sol volume was washed twice with 10 mL *N*,*N*-dimethylformamide until a total filtrate volume of 24 mL was collected. The retained volume was analyzed by GC to determine the presence of residual substrate and derived products. Next the retained sol was diluted with 4 mL *N*,*N*-dimethylformamide and this Au^0 suspension was considered as the starting mixture for the second hydrogenation run. The same procedure was followed for the second filtration and the third reuse experiment.

To study the metal retention and the metal deposition on the ultrafiltration membrane, inductively coupled plasma atomic emission spectroscopy (ICP-AES) was applied. To investigate the association of the metal colloids to the membrane surface during the filtrations, the polyimide membrane was first used in a metal sol filtration and subsequently digested in *aqua regia*, after which the obtained solution was analyzed with a ICP-OES 3300DV apparatus. The metal retention (*R*, %) represents the efficiency of the membrane to retain the metal colloids while the metal association (*A*, %) stands for the fraction of the metal colloids deposited on the membrane after the filtration procedure.

3. Results and discussion

Lower alcohols like ethanol and 2-propanol are widely applied as solvents in the hydrogenation of α,β-unsaturated aldehydes. Therefore, these solvents were tested initially in the crotonaldehyde (**1a**) hydrogenation with polyvinylpyrrolidone (PVP) stabilized Au^0 sols. $HAuCl_4{\cdot}3H_2O$ was used as the gold precursor and a synthesis PVP/Au ratio of 9 was applied as it resulted in acceptable, though moderate colloidal stability of the alcoholic Au^0 sols. As shown in Table 1, both the primary alcohol ethanol and the secondary alcohol 2-propanol led to substantial side product formation through acetalization of the aldehydes (Scheme 1). Up to 14% of acetalization side products were formed in ethanol, and 6% in 2-propanol. As an alternative solvent, 2-butanol was employed [33]. As 2-butanol is less acidic and more sterically hindered, a suppression of the acetalization was expected. The use of 2-butanol indeed led to a nearly complete inhibition of (hemi)acetal formation in the crotonaldehyde hydrogenation, but also to a lower hydrogenation rate and C=O reduction chemoselectivity in comparison with the use of ethanol. Under otherwise identical conditions, the yield of crotyl alcohol (**1b**) was higher in ethanol than in 2-butanol at comparable crotonaldehyde conversion levels. Therefore, 2-butanol is not a worthy alternative for other alcohols.

Next, other polar solvents were screened. Of these, amides like *N*,*N*-dimethylacetamide (DMA) and *N*,*N*-dimethylformamide (DMF) proved most appropriate, both in the synthesis of the Au^0 sol and in its application in the crotonaldehyde hydrogenation. First the amides may help in dissolving the metal precursors by complex formation, either with

Table 1
Effect of the applied solvent and metal on the hydrogenation of crotonaldehyde **1a**

Solvent	Metal precursor	Time (h)	$C_{unsat\ carb}$ (%)	$S_{all\ alc.}$ (%)	$S_{acetal.}$ (%)	$Y_{all\ alc.}$ (%)
Ethanol	$HAuCl_4{\cdot}3H_2O$	40	91	55	14	50
	K_2PtCl_4	18	94	18	11	17
	$RuCl_3{\cdot}xH_2O$	32	92	48	7	44
2-Propanol	$HAuCl_4{\cdot}3H_2O$	48	94	51	6	48
	K_2PtCl_4	24	92	13	5	12
	$RuCl_3{\cdot}xH_2O$	36	92	46	4	42
2-Butanol	$HAuCl_4{\cdot}3H_2O$	48	90	50	<1	45
	K_2PtCl_4	24	91	11	<1	10
	$RuCl_3{\cdot}xH_2O$	36	90	45	<1	41
N,*N*-Dimethyl-acetamide	$HAuCl_4{\cdot}3H_2O$	56	95	66	–	63
	K_2PtCl_4	24	94	16	–	15
	$RuCl_3{\cdot}xH_2O$	32	93	51	–	47
N,*N*-Dimethyl-formamide	$HAuCl_4{\cdot}3H_2O$	48	93	71	–	66
	K_2PtCl_4	30	91	23	–	21
	$RuCl_3{\cdot}xH_2O$	36	91	46	–	42

Reaction conditions: PVP/metal = 9, **1a**/metal = 200, 4.0 MPa H_2, 323 K.

low-molecular amide solvent molecules, or with the amide groups in the PVP polymer [34,35]. Moreover, the high affinity of the amide solvents for the PVP promotes chain unfolding, leading to an improved protective interaction with the metallic surface. The excellent preservation of the Au nanodispersion in amides was proven by TEM analysis (Fig. 1A and B). Alcoholic gold sols on the other hand displayed colloidal instability, as evidenced by a gradual shift of the SPR band to higher wavelengths, and by settling of a phase enriched with colloidal gold when longer preservation or use at temperatures above room temperature were attempted. The amidic sols were the only ones to keep their dispersion and catalytic performance upon storage, as well as under reaction and recycling conditions.

Moreover, the use of amide solvents improves the hydrogenation chemoselectivity. Obviously, there is no acetalization in amides. The selectivity to crotyl alcohol was substantially higher in amides than in ethanol, which was the best alcohol solvent. With Au^0 colloids (PVP/Au = 9) reduced and applied in *N*,*N*-dimethylformamide, crotyl alcohol was obtained with a selectivity exceeding 70% at a crotonaldehyde conversion above 90% (Table 1).

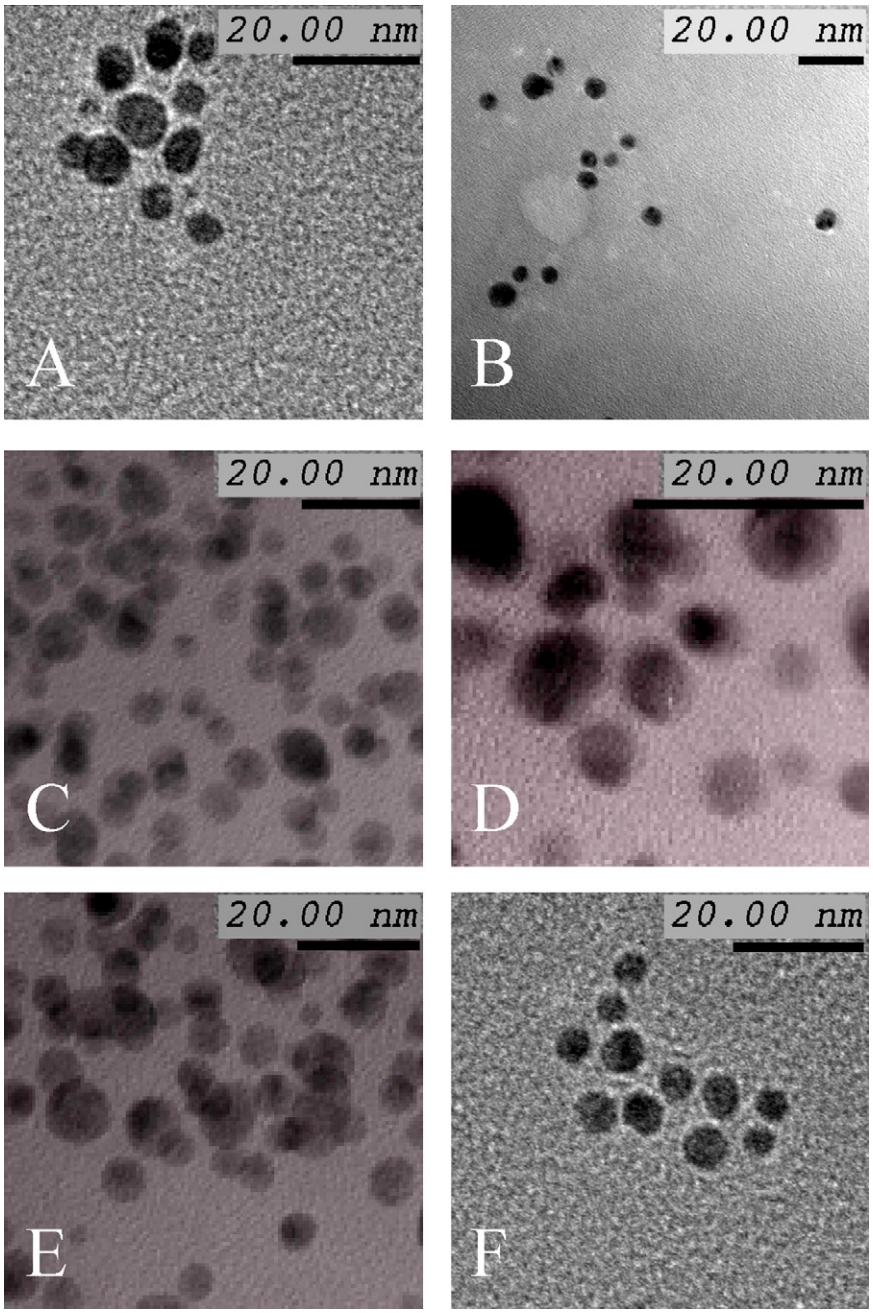

Fig. 1. Transmission electron micrographs of: (A) the optimized Au/DMF sol ($HAuCl_4{\cdot}3H_2O$, PVP/Au = 6), (B) the same optimized Au/DMF sol ($HAuCl_4{\cdot}3H_2O$, PVP/Au = 6) after storage for 28 days, (C) a Au/DMF sol ($AuCl_3$, PVP/Au = 6) with different gold precursor, (D) a Au/DMF sol with more PVP ($HAuCl_4{\cdot}3H_2O$, PVP/Au = 9), (E) a Au/DMF sol with less PVP ($HAuCl_4{\cdot}3H_2O$, PVP/Au = 4.5) and (F) the optimized Au/DMF sol ($HAuCl_4{\cdot}3H_2O$, PVP/Au = 6) after use in the recycling experiments.

For comparison, crotonaldehyde hydrogenations were also performed with Au^0 nanocolloids derived from $AuCl_3$, and with sols synthesized with K_2PtCl_4 and $RuCl_3{\cdot}xH_2O$ as the metal precursors (Table 1). As the variations of the PVP/metal ratio result in different metal cluster sizes (cf. infra), and as the catalytic performance of the metal clusters is size-dependent, a high throughput screening of colloids with different metal identity and cluster size was performed. A limited size-dependency of the hydrogenation chemoselectivity was observed for the various metals while the activity was pronouncedly more size-dependent. In all crotonaldehyde hydrogenation experiments the chemoselectivities observed for Au^0 colloids derived from $HAuCl_4{\cdot}3H_2O$ were slightly superior in comparison with those obtained using $AuCl_3$, irrespective of the PVP/metal ratios and the ensuing cluster sizes (data not shown). Note that for the same reduction conditions, size differences in sols derived from $HAuCl_4{\cdot}3H_2O$ or $AuCl_3$ are negligible (Fig. 1A and C). The Pt^0 colloids were in general highly active, but mainly catalyzed the C=C hydrogenation leading to butanal (**1c**). Ru^0 colloids led to a moderate allylic alcohol selectivity, which is however markedly lower than for the Au^0 counterparts. Thus, Au seems intrinsically more suitable for the chemoselective formation of crotyl alcohol than the widely used metals Pt and Ru. For the further investigations, the catalyst scope will be confined to the Au^0 colloids derived from $HAuCl_4{\cdot}3H_2O$ and dispersed in *N*,*N*-dimethylformamide.

The optimum cluster size of the Au^0 colloids obtained using $HAuCl_4{\cdot}3H_2O$ as the metal precursor was determined with the maximization of the crotyl alcohol yield as the objective. Variation of the PVP/Au ratio influences the cluster size, and thus the selectivity. The evolution of conversion, selectivity, yield and SPR maximum wavelength are given in Table 2. As the PVP/Au ratio is increased, the Au^0 cluster size decreases, and the SPR maximum shifts to shorter wavelengths, even if changes are limited at PVP/Au ratios above 6 [29]. At the optimum, the PVP/Au ratio amounts to 6; based on TEM, these Au^0 colloids have a mean diameter d_{Au} of 7 nm (Fig. 1A).

In comparison with the optimum Au sol, addition of extra protective colloid hardly leads to any further decrease of the cluster size, as evidenced by UV–vis measurements and by TEM (Fig. 1D). Au^0 sols synthesized with PVP/Au ratios higher than the optimum value display lower activity while the hydrogenation chemoselectivity remains almost unaltered (Table 2). This decline in catalytic activity may be ascribed to diffusion limitation in proximity of the metal surface, or to blocking of catalytic sites by sorption of the polymers on the metal surface. PVP/metal ratios lower than 6 on the other hand lead to larger cluster sizes, with markedly lower hydrogenation activities and slightly lower chemoselectivity (Fig. 1E).

Table 2
Effect of the molar PVP/Au ratio of the Au/DMF catalyst on the UV–vis spectrum of the Au sol and the hydrogenation of crotonaldehyde **1a**

$PVP_{monomeric}$/Au (mol/mol)	Max_{SPR} (nm)	$C_{unsat\ carb}$ (%)	$S_{all\ alc.}$ (%)	$Y_{all\ alc.}$ (%)
1.5	574	19	72	14
3.0	558	22	72	16
4.5	544	26	73	19
6	535	27	76	21
9	530	25	76	19
13.5	528	23	76	17
18	524	20	77	15

Reaction conditions: $HAuCl_4{\cdot}3H_2O$, DMF, **1a**/Au = 200, 4.0 MPa H_2, 323 K, 5 h.

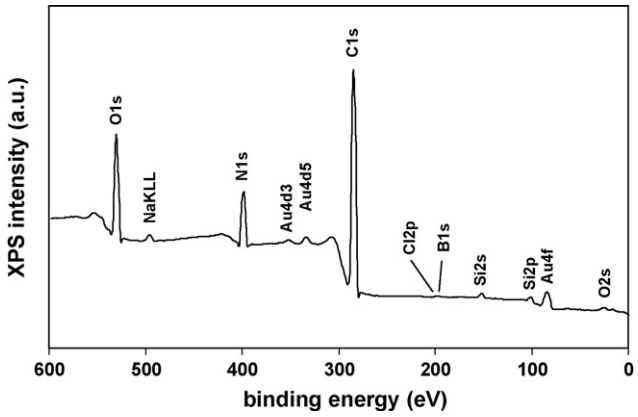

Fig. 2. X-ray photoelectron survey spectrum of the as-prepared Au sol immobilized on glass with C1s at 284.6 eV taken as binding energy reference.

To gain insight into the true chemical nature of the Au^0 nanocolloids the sols were additionally characterized by XPS. Fig. 2 shows the XPS overview spectrum for the optimized gold colloids deposited on glass. Intense lines are readily identified as O1s, C1s and N1s of the organic constituents of the gold sol, more specifically of the solvent *N*,*N*-dimethylformamide and the protective polymer polyvinylpyrrolidone. In addition, weaker signals appear that can be ascribed to the Au4f and 4d core lines, NaKLL (Auger line) as well as to Si2s and Si2p belonging to the glass substrate. Cl2p and B1s are only faintly distinguished in the survey (E_b = 197.5 and 191 eV, respectively). In the XPS high resolution window (Fig. 3), the gold 4f doublet is nicely resolved into its two components. Cl2p and B1s are still weak but do rise above the noise level. After determination of the atomic concentrations, following ratios of Au to other sol elements are obtained: Au/B = 1.39, Au/Cl = 3.22 and Au/Na = 0.74. The $Au4f_{7/2}$ core level is situated at a binding energy of 83.2 eV (with reference to C1s at 284.6 eV). This low position is indicative for gold in its metallic state. No lines were observed pointing to the potential presence of gold boron alloys or gold chloride salts [36].

In Table 3, the effect of the reaction temperature on the hydrogenation of crotonaldehyde over the optimum Au^0 nanocolloids is reported. Apart from an increase in total hydrogenation rate, a higher temperature might change the intramolecular hydrogenation competition because of the different activation energies for the hydrogenation of the C=C and C=O bonds [37]. Conversion levels, measured at short reaction times, were almost doubled by a 40 K temperature rise. Obviously this rate increase is too small for a thermally activated chemical reaction. Slow diffusion of the substrate through the protective shell around the gold nanoclusters might play a role in the unexpectedly small thermal activation, as discussed previously. The hydrogenation chemoselectivity was

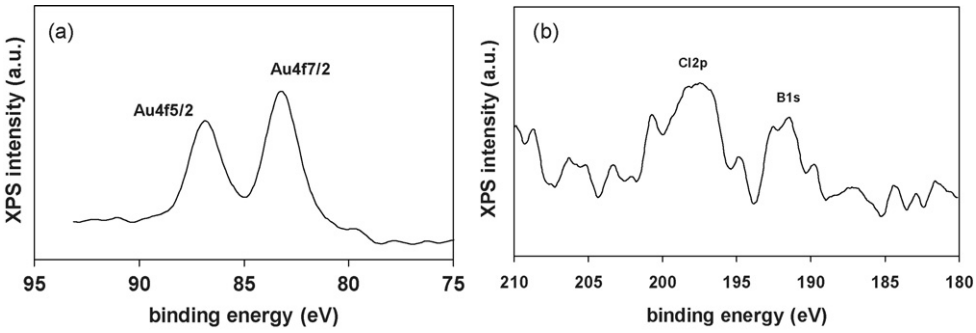

Fig. 3. X-ray photoelectron spectrum of the Au4f doublet signal (A) and Cl2p and B1s window (B) for the as-prepared Au sol, immobilized on glass.

only slightly affected by the temperature variation, with changes of less than 5% at equal crotonaldehyde conversion levels. In view of the long term performance of the Au^0 colloids, 333 K emerged as the optimum temperature, because of a decreased colloidal stability of the gold catalyst at higher temperatures and a gradual deactivation in the course of the reaction. Variations in H_2 pressure in the 0.5–4.0 MPa range had no pronounced effect on the course of the crotonaldehyde hydrogenation.

In order to understand the reaction network, the reactivities of crotonaldehyde (**1a**) and the primary hydrogenation products crotyl alcohol (**1b**) and butanal (**1c**) were compared in the optimum hydrogenation conditions. The reactivity of crotonaldehyde was about twice that of butanal while the reactivity of crotyl alcohol was remarkably low. The low crotyl alcohol reactivity definitely accounts for the limited decline in chemoselectivity over a wide crotonaldehyde conversion range. The initial crotonaldehyde hydrogenation step, leading to either crotyl alcohol or butanal, is clearly decisive for the hydrogenation chemoselectivity. A second hydrogenation step mainly occurs for butanal, and leads only to a variation in the distribution of the unwanted hydrogenation products butanal and 1-butanol.

Next, the optimized Au^0 sol was applied in the hydrogenation of the α,β-unsaturated ketone mesityl oxide (**2a**). The allylic alcohol selectivity was 64% at 91% mesityl oxide conversion (Table 4). Under identical, initial hydrogenation conditions the reactivity of crotonaldehyde was at least twice that of mesityl oxide (data not shown). This decline in substrate reactivity is presumably related to the methyl substitution on the carbonyl group, which hampers or changes the substrate adsorption on the catalytic surface. The additional alkyl group in a α,β-unsaturated ketone in comparison to a α,β-unsaturated aldehyde changes the adsorption conformation, and makes the molecule less susceptible to chemoselective C=O reduction [38].

To gain further insight in the effects of α- or β-substitution of the C=C–C=O group, the results obtained with crotonaldehyde (**1a**) and mesityl oxide (**2a**) were compared with those obtained with methacrolein (**3a**) and 3-methyl-3-penten-2-one (**4a**). For both α,β-unsaturated aldehydes and ketones, this implies a shift of one methyl group from the β-position to the α-position on the C=C bond. As reported in Table 4, the hydrogenation of methacrolein was slightly slower compared to that of crotonaldehyde, but formation of methallyl alcohol (**3b**) was slightly more selective at equal conversion levels. For the α,β-unsaturated ketones, the substrate with the α-substitution, viz. 3-methyl-3-penten-2-one (**4a**), was again hydrogenated at a lower rate, but with a higher chemoselectivity for C=O hydrogenation. An allylic alcohol selectivity of 70% was attained at 90% 3-methyl-3-penten-2-one conversion. Clearly, methyl substitution on the α-position of the C=C bond is more advantageous for the hydrogenation chemoselectivity than β-substitution.

Table 3
Effect of the reaction temperature on the hydrogenation of crotonaldehyde **1a**

Temperature (K)	Time (h)	$C_{unsat\ carb}$ (%)	$S_{all\ alc.}$ (%)	$Y_{all\ alc.}$ (%)
303	5	16	73	12
313	5	22	74	16
323	5	26	76	20
333	5	29	78	23
343	5	31	78	24
303	56	92	70	64
313	50	93	70	65
323	44	92	72	66
333	40	93	73	68
343	40	91	74	67

Reaction conditions: $HAuCl_4{\cdot}3H_2O$, DMF, PVP/Au = 6, **1a**/Au = 200, 4.0 MPa H_2.

Table 4
Comparative study on substrate reactivity and hydrogenation chemoselectivity

Substrate		Time (h)	$C_{unsat\ carb}$ (%)	$S_{all\ alc.}$ (%)	$S_{sat\ carb.}$ (%)	$S_{sat\ alc.}$ (%)
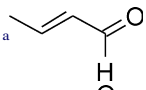 [a]	**1a**	40	92	73	5	22
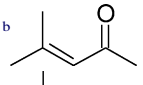 [b]	**2a**	48	91	64	8	28
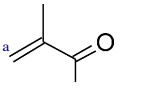 [a]	**3a**	48	93	75	4	21
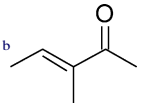 [b]	**4a**	56	90	70	7	23

Reaction conditions: $HAuCl_4{\cdot}3H_2O$, DMF, PVP/Au = 6, 4.0 MPa H_2, 333 K.
[a] Substrate/Au = 200.
[b] Substrate/Au = 100.

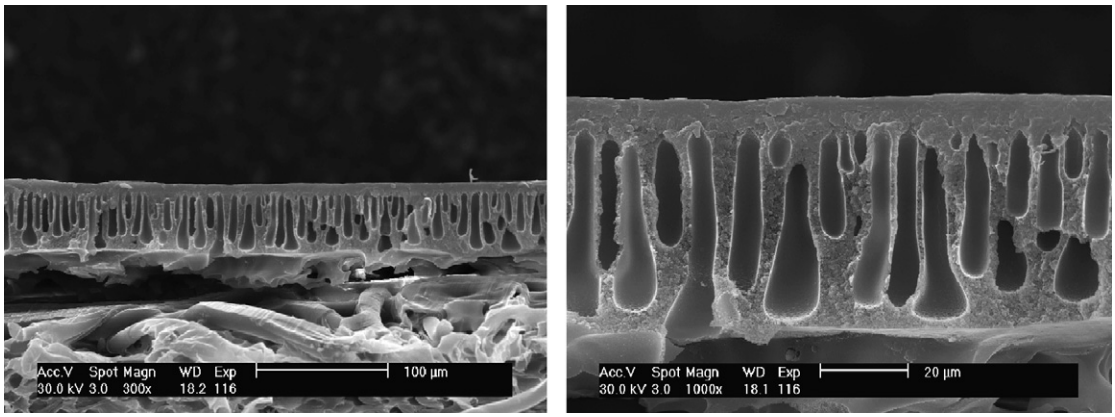

Fig. 4. Scanning electron micrographs of the optimum cross-linked polyimide membrane.

Finally, recycling of the colloidal Au^0 nanocatalyst was attempted by ultrafiltration. The custom-made polyimide membranes as such proved chemically unstable in amides and dissolved partially. By a post-synthesis cross-linking treatment the polyimide membranes became solvent-resistant and usable for the separation of the colloidal gold catalyst from the amidic reaction mixtures. In the cross-linking procedure the imide groups of the PI chains are partly substituted by amidic bonds via opening of the imide rings with *p*-xylylenediamine. The evolution of the cross-linking was followed by DRIFTS. Comparison of a non-treated PI membrane with membrane samples cross-linked for different times showed a gradual increase of the signal around 3250 cm^{-1}, characteristic for N–H stretching vibrations. To study the physical nature of the cross-linked polyimide membranes, SEM pictures of membrane cross-sections were made (Fig. 4). The PI layer measured about 50 μm with a denser top zone of about 10 μm and with abundant macrovoids in the underlying 40 μm layer. This is typical for polymer membranes synthesized via the phase-inversion technique.

Preliminary ultrafiltration experiments over the solvent-resistant PI membranes indicated that organic compounds like the substrate and the various hydrogenation products migrate freely through the membrane with the solvent flow as the organic composition of the retentate and filtrate fractions was nearly identical. Regarding the sol separation, a >99% retention *R* of the colloidal Au^0 catalyst was achieved, while the association of Au species *A* on the ultrafiltration membrane was below 1% as determined by ICP-AES.

Also in the recycling experiments and after multiple use the cross-linked PI membrane retained the Au^0 nanocolloids effectively, which allowed an efficient catalyst separation from the reaction mixtures. During the filtration of reaction mixtures no 'fouling' association of mixture compounds with the modified PI membrane was observed. The colloidal Au^0 catalyst maintained at least 90% of its inceptive activity in the third crotonaldehyde hydrogenation run as shown in Table 5. Moreover, no change in the hydrogenation chemoselectivity was observed indicating that the specific properties of the optimum Au^0 nanocolloids were not altered during the hydrogenation reaction. This is in agreement with the stability of the gold sol, as observed via TEM (Fig. 1F). These observations prove the satisfactory and durable catalytic performance of the polyvinylpyrrolidone stabilized Au^0 nanoparticles in the hydrogenation of α,β-unsaturated aldehydes and ketones.

Table 5
Recycling experiment on crotonaldehyde **1a** hydrogenation by Au^0 nanocolloids

Run	$C_{unsat\ carb}$ (%)	$S_{all\ alc.}$ (%)	$S_{sat\ carb.}$ (%)	$S_{sat\ alc.}$ (%)	$Y_{all\ alc.}$ (%)
1	97	70	5	25	68
2	92	73	5	22	67
3	89	74	7	21	66

Reaction conditions: $HAuCl_4 \cdot 3H_2O$, DMF, PVP/Au = 6, **1a**/Au = 100, 4.0 MPa H_2, 333 K, 24 h.

4. Conclusions

Polyvinylpyrrolidone stabilized Au^0 nanocolloids dispersed in amides display a high chemoselectivity in the hydrogenation of both α,β-unsaturated aldehydes and ketones to allylic alcohols. Analogous Pt^0 and Ru^0 nanocolloids are more active than their Au^0 counterparts, but substantially less chemoselective for allylic alcohols. Experimental control over the Au^0 cluster generation provided the opportunity to investigate the size-dependency of the catalytic performance of nano-Au^0 and to determine the optimum gold cluster size leading to the highest allylic alcohol yields. The intrinsic reactivity of α,β-unsaturated ketones is lower than that of analogous α,β-unsaturated aldehydes. Methyl substitution on the α-position of the C=C bond favors selective allylic alcohol formation. The Au^0 nanocolloids can be recycled effectively by ultrafiltration using a cross-linked polyimide membrane, which is chemically stable in amides. In this way the durable Au^0 nanosols could efficiently be reused with satisfactory preservation of the catalytic performance.

Acknowledgements

P. Mertens is grateful to IWT for a PhD fellowship. D. De Vos thanks F.W.O. for a research grant on high throughput catalysis. This work was performed in the framework of the

Belgian Programme on Interuniversity Poles of Attraction initiated by the Belgian State, Prime Minister's Office, Science Policy Programming (IAP-V/03). We acknowledge Ulric Demeter for XPS measurements.

References

[1] K. Bauer, D. Garbe, H. Surburg, Common Fragrance and Flavour Materials, Wiley–VCH, Weinheim, 1997.
[2] P. Kraft, J.A. Bajgrowicz, C. Denis, G. Fráter, Angew. Chem. 112 (2000) 3106.
[3] Ullmann's Encyclopedia of Technical Chemistry, Electronic Release, 6th ed., Wiley–VCH, 2000.
[4] M. Okumura, T. Akita, M. Haruta, Catal. Today 74 (2002) 265.
[5] S. Schimpf, M. Lucas, C. Mohr, U. Rodemerck, A. Brückner, J. Radnik, H. Hofmeister, P. Claus, Catal. Today 72 (2002) 63.
[6] G.C. Bond, P.A. Sermon, G. Webb, D.A. Buchanan, P.B. Wells, J. Chem. Soc. Chem. Commun. (1973) 444.
[7] A. Corma, P. Serna, Science 313 (2006) 332.
[8] Y. Chen, J. Qiu, X. Wang, J. Xiu, J. Catal. 242 (2006) 227.
[9] C. Mohr, H. Hofmeister, P. Claus, J. Catal. 213 (2003) 86.
[10] C. Mohr, H. Hofmeister, J. Radnik, P. Claus, J. Am. Chem. Soc. 125 (2003) 1905.
[11] P. Claus, A. Brückner, C. Mohr, H. Hofmeister, J. Am. Chem. Soc. 122 (2000) 11430.
[12] B. Campo, M. Volpe, S. Ivanova, R. Touroude, J. Catal. 242 (2006) 162.
[13] R. Zanella, C. Louis, S. Giorgio, R. Touroude, J. Catal. 223 (2004) 328.
[14] J.J. Bailie, G.J. Hutchings, J. Chem. Soc. Chem. Commun. (1999) 2151.
[15] J.E. Baillie, H.A. Abdullah, J.A. Anderson, C.H. Rochester, N.V. Richardson, N. Hodge, J.-G. Zhang, A. Burrows, C.J. Kiely, G.J. Hutchings, Phys. Chem. Chem. Phys. 3 (2001) 4113.
[16] C. Milone, M.L. Tropeano, G. Gulino, G. Neri, R. Ingoglia, S. Galvagno, J. Chem. Soc. Chem. Commun. (2002) 868.
[17] C. Milone, R. Ingoglia, M.L. Tropeano, G. Neri, F. Frusteri, S. Galvagno, J. Chem. Soc. Chem. Commun. (2003) 868.
[18] C. Milone, R. Ingoglia, A. Pistone, G. Neri, F. Frusteri, S. Galvagno, J. Catal. 222 (2004) 348.
[19] C. Milone, R. Ingoglia, L. Schipilliti, C. Crisafulli, G. Neri, S. Galvagno, J. Catal. 236 (2005) 80.
[20] M. Comotti, C. Della Pina, R. Materrese, M. Rossi, Angew. Chem. Int. Ed. 116 (2004) 5936.
[21] P.G.N. Mertens, M. Bulut, L.E.M. Gevers, I.F.J. Vankelecom, P.A. Jacobs, D.E. De Vos, Catal. Lett. 102 (2005) 57.
[22] P.G.N. Mertens, I.F.J. Vankelecom, P.A. Jacobs, D.E. De Vos, Gold Bull. 38 (2005) 157.
[23] A. Mirescu, U. Prüβe, Catal. Commun. 7 (2006) 11.
[24] W. Yu, Y. Wang, H. Liu, W. Zheng, J. Mol. Catal. A 112 (1996) 105.
[25] W. Yu, H. Liu, M. Liu, Q. Tao, J. Mol. Catal. A 138 (1999) 273.
[26] W. Yu, H. Liu, M. Liu, Z. Liu, React. Funct. Polym. 44 (2000) 21.
[27] P.S. Tin, T.S. Chung, Y. Liu, R. Wang, S.L. Liu, K.P. Pramoda, J. Membr. Sci. 225 (2003) 77.
[28] J.P. Wilcoxon, R.L. Williamson, R. Baughman, J. Phys. Chem. 98 (1993) 9933.
[29] A. Slistan-Grijalva, R. Herrera-Urbina, J.F. Rivas-Silva, M. Avalos-Borja, F.F. Castillon-Barraza, A. Posada-Amarillas, Physica E 27 (2005) 104.
[30] J.L. Margitfalvi, A. Tompos, I. Kolosova, J. Valyon, J. Catal. 174 (1998) 246.
[31] J.L. Luche, J. Am. Chem. Soc. 100 (1978) 2226.
[32] J.L. Luche, A.L. Gemal, J. Am. Chem. Soc. 101 (1979) 5848.
[33] P. Maki-Arvela, L.-P. Tiainen, A.K. Neyestanaki, R. Sjoholm, T.-K. Rantakyla, E. Laine, T. Salmi, D.Y. Murzin, Appl. Catal. A 237 (2002) 181.
[34] C. Comuzzi, P. Di Bernardo, P. Polese, R. Portanova, M. Tolazzi, P.L. Zanonato, Polyhedron 19 (2000) 2427.
[35] J.H. Kim, B.R. Min, J. Won, Y.S. Kang, J. Polym. Sci. Part B: Polym. Phys. 44 (2006) 1168.
[36] Handbook of X-ray Photoelectron Spectroscopy, Physical Electronics. http://www.phi.com.
[37] U.K. Singh, M.A. Vannice, J. Catal. 191 (2000) 165.
[38] V. Ponec, Appl. Catal. A 149 (1997) 27.